Cancer Research

AIMP2 Controls Intestinal Stem Cell Compartments and Tumorigenesis by Modulating Wnt/β-Catenin Signaling

Min Kyu Yum[1], Jong-Seol Kang[1], Al-Eum Lee[2], Young-Woo Jo[1], Ji-Yun Seo[1], Hyun-A Kim[1], Yoon-Young Kim[1], Jinwoo Seong[1], Eun Byul Lee[1], Ji-Hoon Kim[1], Jung Min Han[3,4], Sunghoon Kim[2,5,6], and Young-Yun Kong[1]

Abstract

Wnt/β-catenin (CTNNB1) signaling is crucial for the proliferation and maintenance of intestinal stem cells (ISC), but excessive activation leads to ISC expansion and eventually colorectal cancer. Thus, negative regulators are required to maintain optimal levels of Wnt/β-catenin signaling. Aminoacyl-tRNA synthetase–interacting multifunctional proteins (AIMP) function in protein synthesis, but have also been implicated in signaling cascades affecting angiogenesis, immunity, and apoptosis. In this study, we investigated the relationship between AIMP2 and Wnt/β-catenin signaling in a murine model of intestinal homeostasis and tumorigenesis. Hemizygous deletion of *Aimp2* resulted in enhanced Wnt/β-catenin signaling, increased proliferation of cryptic epithelial cells, and expansion of ISC compartments. In an $Apc^{Min/+}$ background, *Aimp2* hemizygosity increased adenoma formation. Mechanistically, AIMP2 disrupted the interaction between AXIN and Dishevelled-1 (DVL1) to inhibit Wnt/β-catenin signaling by competing with AXIN. Furthermore, AIMP2 inhibited intestinal organoid formation and growth by suppressing Wnt/β-catenin signaling in an *Aimp2* gene dosage-dependent manner. Collectively, our results showed that AIMP2 acts as a haploinsufficient tumor suppressor that fine-tunes Wnt/β-catenin signaling in the intestine, illuminating the regulation of ISC abundance and activity. *Cancer Res; 76(15); 4559–68. ©2016 AACR.*

Introduction

The intestinal epithelium self-renews every 3 to 5 days through its highly proliferative compartment, the crypt of Lieberkühn. Intestinal stem cells (ISC) expressing leucine-rich repeat-containing G-protein–coupled receptor 5 (LGR5) residing at the bottom of crypts generate all types of cells in the intestinal epithelium (1). Cryptal mesenchymal cells and Paneth cells (PC) constitute the ISC niche and support the maintenance of ISCs by producing factors such as EGF, Notch, and Wnt (2).

Wnt/β-catenin signaling plays a pivotal role in homeostatic self-renewal of ISCs (3). Binding of Wnt ligands to its receptors, Frizzled and low-density lipoprotein receptor–related protein 5/6 (LRP5/6) activate a signaling cascade inhibiting the β-catenin destruction complex, which contains axis inhibition protein (AXIN), adenomatous polyposis coli (APC), and glycogen synthetase kinase 3β (GSK3β). β-catenin subsequently accumulates and translocates to the nucleus, forming a complex with T-cell–specific transcription factor/lymphoid enhancer–binding factor family to control target gene expressions (4), which supports the maintenance, proliferation, and differentiation of ISCs.

Disruption of Wnt/β-catenin signaling leads to ISC depletion and crypt degeneration (5, 6). Conversely, constitutive activation of Wnt/β-catenin signaling in the intestinal epithelium drives excessive cell proliferation and tumor formation (7). Approximately 80% of human sporadic colorectal tumors are caused by mutations in the *APC* gene, and mice lacking the *Apc* gene in ISCs develop severe polyposis (8). These studies suggest that the activity of Wnt/β-catenin signaling should be tightly regulated, albeit ISCs require Wnt/β-catenin signaling to maintain their stemness. Interestingly, despite abundant sources of Wnt ligands at the crypt base (9), Wnt/β-catenin signaling is not fully activated in ISCs. Recently, Koo and colleagues reported that the RNF43 and ZNRF3 E3 ligases ubiquitinate Wnt receptors and inhibit Wnt/β-catenin signaling (10). Importantly, *Rnf43/Znrf3* compound–mutant mice show increased intestinal proliferation and eventually develop adenomas that phenocopy the *Apc*-mutant mice (8), suggesting that inhibition of Wnt/β-catenin signaling by RNF43 and ZNRF3 is critical for suppressing ISC proliferation. Nevertheless, *Rnf43/Znrf3*–mutant adenomas showed low-grade characteristics, including smaller adenoma size and less abrogated epithelial structure when compared with *Apc*-mutant mice. These differences suggest that additional regulatory mechanisms exist between the Wnt receptor and the β-catenin destruction complex.

The aminoacyl-tRNA synthetases (ARS) are catalytic enzymes that attach specific amino acids to their corresponding tRNAs. Eight different ARSs form the multi-tRNA synthetase complex

[1]Department of Biological Sciences, Seoul National University, Seoul, South Korea. [2]College of Pharmacy, Seoul National University, Seoul, South Korea. [3]Department of Integrated OMICS for Biomedical Science, Yonsei University, Seoul, South Korea. [4]College of Pharmacy, Yonsei University, Incheon, South Korea. [5]Medicinal Bioconvergence Research Center, Seoul National University, Seoul, Republic of Korea. [6]Department of Molecular Medicine and Biopharmaceutical Sciences, Seoul National University, Seoul, South Korea.

Note: Supplementary data for this article are available at Cancer Research Online (http://cancerres.aacrjournals.org/).

Corresponding Author: Young-Yun Kong, Department of Biological Sciences, Seoul National University, 599 Gwanak-ro, Gwanak-gu, Seoul 151-747, South Korea. Fax: 822-872-1993; E-mail: ykong@snu.ac.kr

doi: 10.1158/0008-5472.CAN-15-3357

associating with three nonenzymatic ARS-interacting multifunctional proteins (AIMP), AIMP1, AIMP2, and AIMP3, which stabilize the assembly of ARSs into the multi-tRNA synthetase complex (11). Despite "housekeeping" functions of ARSs and AIMPs in protein synthesis, accumulating evidence indicates they have noncanonical functions beyond protein synthesis (12). For instance, after genotoxic stress, AIMP3 translocates to the nucleus activating p53 through the activation of the kinases ataxia telangiectasia mutated (ATM) and ATM- and Rad3-related (ATR; ref. 13). Some ARSs and AIMPs, such as tyrosyl-tRNA synthetase and AIMP1, are secreted as extracellular signaling factors controlling angiogenesis and immune responses (14, 15). AIMP2 is also involved in other signaling pathways besides amino-acylation. Genetic disruption of *Aimp2* results in neonatal lethality by defects in lung differentiation (16). It has also been reported that AIMP2 induces apoptosis by promoting the degradation of TNF-receptor associated factor 2 (TRAF2) and the activation of p53 in response to DNA damage (17, 18). Interestingly, the activity of AIMP2 seems highly sensitive to *Aimp2* gene dosage, suggesting that the level of AIMP2 is important for its roles as a signaling modulator (19).

Here, we investigated the effect of AIMP2 haploinsufficiency in the intestinal epithelium and tumorigenesis using mouse models and an organoid culture system. We found that hemizygous deletion of the *Aimp2* gene enhanced the initiation of intestinal adenoma formation in $Apc^{Min/+}$ mice. AIMP2 was highly expressed in the crypt compared with the villus, and hemizygous deletion of *Aimp2* led to the expansion of ISCs and PCs, which constitute the ISC compartment. Consistently, the expression of Wnt target genes were markedly increased in $Aimp2^{+/-}$ intestines compared with $Aimp2^{+/+}$. At the mechanistic level, AIMP2 bound to Dishevelled (DVL) and disrupted DVL–AXIN interaction, thereby inhibiting Wnt/β-catenin signaling. Importantly, *in vitro* and organoid formation analyses using $Aimp2^{+/+}$, $Aimp2^{+/-}$, and $Aimp2^{-/-}$ mouse embryonic fibroblasts (MEF) and intestinal epithelial cells (IEC), respectively, showed that the activity of Wnt/β-catenin signaling negatively correlated with *Aimp2* gene dosage. Collectively, our results reveal a pivotal role for AIMP2 in fine-tuning of Wnt/β-catenin signaling activity in the intestinal epithelium.

Materials and Methods

Mice

The $Apc^{Min/+}$ and the *Lgr5-EGFP-IRES-CreERT2* (*Lgr5-EGFP*) mice were purchased from Jackson Laboratories. The generation of *Aimp2*-mutant mice has been described elsewhere (20). The *Aimp2*-mutant mice had been backcrossed at least eight times onto the C57BL/6J backgrounds. $Apc^{Min/+}$ mice were interbred with $Aimp2^{+/-}$ mice to generate $Aimp2^{+/+}$:$Apc^{Min/+}$ and $Aimp2^{+/-}$:$Apc^{Min/+}$ littermates. All animal experiments were performed in accordance with the guidelines of Seoul National University Institutional Animal Care and Use Committee.

Histopathologic analysis

For assessment of polyposis in $Apc^{Min/+}$ mice, intestine segments were subdivided into four segments (duodenum, jejunum, ileum, and colon), flushed with PBS, and opened longitudinally onto 3 mm paper or embedded in paraffin wax. The tissues were fixed overnight at 4°C in 4% paraformaldehyde. Adenomas were stained with methylene blue and analyzed with the aid of dissecting microscope (Zeiss). For detailed histologic analysis, sections were stained with hematoxylin & eosin (H&E) or periodic acid–Schiff (PAS)/hematoxylin (H).

Immunofluorescence

The intestinal tract was flushed with cold PBS, followed by 4% paraformaldehyde at 4°C, and embedded in paraffin wax for sectioning. The sections (4 μm) were stained with indicated primary antibodies. For detailed information, including primary antibody, see the Supplementary Materials and Methods.

Intestinal epithelium and crypt isolation

Intestinal epithelium and crypt isolation were performed as described previously (21). Briefly, the fragment (4 cm) of the ileum was rinsed with PBS. The fragments were cut into pieces and placed into 50-mL conical tubes filled with cold PBS containing 20 mmol/L EDTA to isolate intestinal epithelium. For detailed information, see the Supplementary Materials and Methods.

Cell culture and *in vitro* reporter assay

All cell lines were obtained from the ATCC in 2015. Upon receipt, cells were frozen, and individual aliquots were taken into culture, for analysis within <10 passages. HCT116, HeLa, HEK, and MEF cells were cultured in medium (HCT116: RPMI 1640, HeLa, HEK, and MEF: DMEM) supplemented with 10% FBS (HyClone), 100 U/mL penicillin, and 100 μg/mL streptomycin in an atmosphere of 95% air and 5% CO_2 at 37°C. ATCC checks the authenticity of these cell lines using short tandem repeat analyses. For reporter assays, cells were transfected with the indicated plasmids. siRNA to *AIMP2* was designed and synthesized by Dharmacon (Thermo Scientific). Luciferase activity was measured using the Dual Luciferase Reporter Assay Kit (Promega).

Coimmunoprecipitation

Coimmunoprecipitation was performed as described previously (17). The cells were lysed in protein lysis buffer (0.1% NP-40, 25 mmol/L Tris, 0.5 mmol/L EGTA, 10 mmol/L NaCl, 0.5 mmol/L $MgCl_2$, 1 mmol/L EDTA, proteinase/phosphatase inhibitor cocktail). The lysates were centrifuged at 12,000 rpm for 30 minutes. The supernatants were immunoprecipitated overnight at 4°C with a normal IgG antibody (Santa Cruz Biotechnology) or a specific mAb, which was preincubated with Protein A/G agarose beads. Beads were washed six times with cold protein lysis buffer. The precipitates were separated by SDS-PAGE. After the proteins were transferred to a polyvinylidene difluoride membrane, coimmunoprecipitation was assessed by immunoblotting.

Organoid culture

Organoid culture has been described previously (22). In brief, freshly isolated crypts were pelleted in Matrigel (BD Biosciences). After Matrigel polymerization, organoid growth medium was added. For detailed information, see the Supplementary Materials and Methods.

Statistical analysis

Statistical significance was determined by applying Student *t* test or ANOVA to raw values from at least three independent experiments. ANOVA was used to evaluate the dependence of a parameter on *Aimp2* gene dosage. Data are as the mean ± SEM. *, $P < 0.01$ was considered statistically significant.

Results

Hemizygous deletion of *Aimp2* in $Apc^{Min/+}$ mice results in enhanced tumor burden

To investigate whether AIMP2 haploinsufficiency affects intestinal tumorigenesis, we crossed $Aimp2^{+/-}$ mice with $Apc^{Min/+}$ mice (23). Interestingly, $Aimp2^{+/-}$:$Apc^{Min/+}$ mice exhibited significantly reduced survival rates when compared with $Aimp2^{+/+}$:$Apc^{Min/+}$ mice (Fig. 1A). Consistently, methylene blue staining of whole intestinal tracts showed that the number of polyps significantly increased in both genders of 20-week-old $Aimp2^{+/-}$:$Apc^{Min/+}$ mice (average 98.4 polyps per mouse) than in $Aimp2^{+/+}$:$Apc^{Min/+}$ littermates (average 62.4 polyps per mouse; Fig. 1B and Supplementary Fig. S1A). Polyp counting on intestinal segments including duodenum, jejunum, ileum, and colon showed general increase of polyp formation in $Aimp2^{+/-}$:$Apc^{Min/+}$ intestine (Fig. 1C). The polyps in $Aimp2^{+/-}$:$Apc^{Min/+}$ mice were notably larger than those in $Aimp2^{+/+}$:$Apc^{Min/+}$ mice (Fig. 1D and Supplementary Fig. S1B). Remarkably, about 50% of the polyps in $Aimp2^{+/-}$:$Apc^{Min/+}$ mice had a diameter larger than 2 mm, compared with 24% of the polyps in $Aimp2^{+/+}$:$Apc^{Min/+}$ mice (Fig. 1E). Although the size of the polyps increased in $Aimp2^{+/-}$:$Apc^{Min/+}$ mice, invading tumors were not detected, even in moribund $Aimp2^{+/-}$:$Apc^{Min/+}$ mice (data not shown).

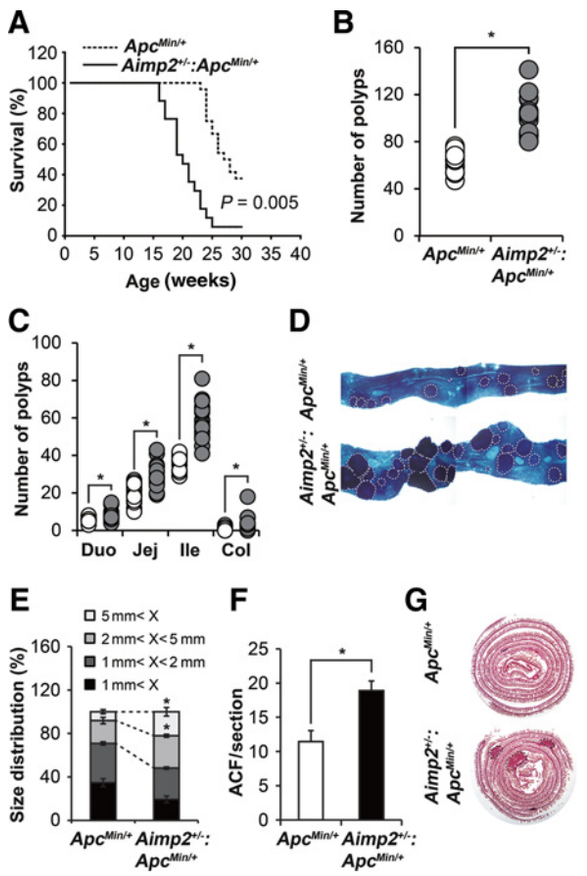

Figure 1.

AIMP2 acts as a haploinsufficient tumor suppressor in $Apc^{Min/+}$ mice. **A,** Kaplan–Meier survival graph of $Aimp2^{+/+}$:$Apc^{Min/+}$ ($n = 24$) and $Aimp2^{+/-}$:$Apc^{Min/+}$ ($n = 17$) littermates. The *P* value is based on the log-rank test. **B** and **C,** polyp numbers in 20-week-old $Aimp2^{+/+}$:$Apc^{Min/+}$ ($n = 23$) and $Aimp2^{+/-}$:$Apc^{Min/+}$ ($n = 24$) whole intestines (**B**) and different intestinal segments (**C**) Duo, duodenum; Jej, jejunum; Ile, ileum; Col, colon. **D,** methylene blue staining of the ileums. The polyps are circled with white dashed lines. **E,** size distribution of polyps in $Aimp2^{+/+}$:$Apc^{Min/+}$ ($n = 6$) and $Aimp2^{+/-}$:$Apc^{Min/+}$($n = 4$) intestine. **F,** numbers of ACF in 6-week-old $Aimp2^{+/+}$:$Apc^{Min/+}$ ($n = 5$) and $Aimp2^{+/-}$:$Apc^{Min/+}$($n = 5$) intestine. One of every five consecutive sections was examined. ACF were quantified in 10 sections. **G,** H&E staining of small intestines from 7-week-old mice. Polyps are circled with black dashed lines. Student *t* test was applied, and data are the mean ± SEM. *, $P < 0.01$.

To investigate whether the increase in polyp number and size in $Aimp2^{+/-}$:$Apc^{Min/+}$ mice were due to earlier tumor initiation, we examined tumor initiation by counting aberrant crypt foci (ACF), the preneoplastic lesions of intestinal tumors (24). Histologic analysis of the whole small intestine from 6-week-old mice showed that the number of ACF increased in $Aimp2^{+/-}$:$Apc^{Min/+}$ mice (average 18.9 ± 3.1 per section) than that in $Aimp2^{+/+}$:$Apc^{Min/+}$ mice (average 11.5 ± 3.6 per section; Fig. 1F and Supplementary Fig. S1C). Consistently, large tumors were readily observed in 7-week-old $Aimp2^{+/-}$:$Apc^{Min/+}$ mice, but not in the littermate controls (Fig. 1G and Supplementary Fig. S1D), indicating that $Aimp2^{+/-}$:$Apc^{Min/+}$ mice had accelerated tumor formation. Collectively, these results suggest that AIMP2 acts as a haploinsufficient tumor suppressor in intestinal tumorigenesis.

Hemizygous deletion of *Aimp2* increases proliferation in the crypts

To investigate a role of AIMP2 in IECs, we examined the expression pattern of AIMP2 in intestine. At embryonic day 18.5, AIMP2 was highly expressed at the intervillus region of $Aimp2^{+/+}$ intestine but not in $Aimp2^{-/-}$ (Fig. 2A), indicating that the antibody is specific to AIMP2. In the adult intestine, AIMP2 was highly expressed in the crypt, where it predominantly localized in the cytosol (Fig. 2B). Consistent with immunohistochemical detection of AIMP2 in crypt, *Aimp2* mRNA expression in the crypt fractions was about 2.5-fold higher than that in the villus fractions (Fig. 2C), suggesting that AIMP2 functions in the crypts.

Because loss of heterozygosity (LOH) in $Apc^{Min/+}$ mice is a stochastic event (25), intestinal tumor formation in $Apc^{Min/+}$ mice depends on the proliferation rate of IECs, including ISCs in which LOH should occur (8). Therefore, we examined whether hemizygous deletion of *Aimp2* affected the proliferation of IECs, including ISCs. The lengths of the crypt and villus were increased in heterozygous $Aimp2^{+/-}$ mice compared with $Aimp2^{+/+}$ (Fig. 2D and Supplementary Fig. S2A and S2B). The number of $Ki67^+$ cells increased in the $Aimp2^{+/-}$ crypts ($Aimp2^{+/+}$: 17.8 ± 4.7 vs. $Aimp2^{+/-}$: 27.4 ± 4.9 per crypt; Fig. 2E and F). To confirm these results, we injected mice with bromodeoxyuridine (BrdUrd) 2 hours before sacrifice and counted BrdUrd-labeled cycling cells. As expected, the number of $BrdUrd^+$ cells significantly increased in the $Aimp2^{+/-}$ crypts ($Aimp2^{+/+}$: 12.3 ± 3.1 vs. $Aimp2^{+/-}$: 19.5 ± 4.4 per crypt; Fig. 2G and H and Supplementary Fig. S2C).

Notably, AIMP2 is also highly expressed in the bottom of the colonic crypts (Supplementary Fig. S2D). The number of $Ki67^+$ cells was also increased in the $Aimp2^{+/-}$ colon ($Aimp2^{+/+}$: 10.7 ± 1.9 vs. $Aimp2^{+/-}$: 17.7 ± 3.2 per crypt; Supplementary Fig. S2E and S2F). TUNEL and cleaved caspase-3 staining revealed that apoptosis of IECs is not affected when AIMP2 is reduced (Fig. 2I and J and Supplementary Fig. S2G and S2H). Taken together, these results suggest that AIMP2 inhibits the proliferation of IECs in the crypts throughout the intestine.

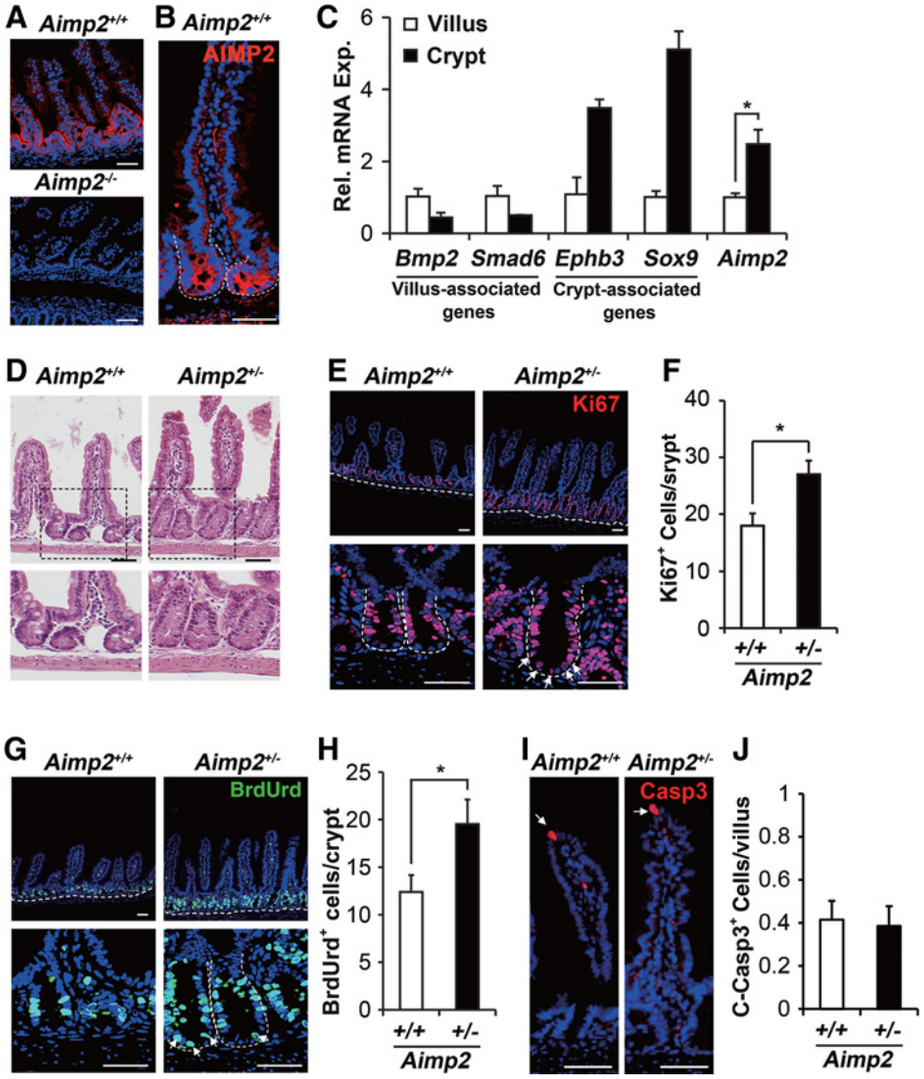

Figure 2.
AIMP2 inhibits epithelial cell proliferation in the intestinal crypt. **A** and **B,** immunohistochemical staining of AIMP2 in E18.5 (**A**) and 20-week-old (**B**) intestine. **C,** mRNA expressions in villi/crypt fractions from wild-type mice ($n = 3$). **D,** representative H&E staining in ileums of 20-week-old *Aimp2*$^{+/+}$ and *Aimp2*$^{+/-}$. **E–H,** immunohistochemical staining and quantification of Ki67 (**E** and **F**) and BrdUrd (**G** and **H**) in ileal crypts of 20-week-old *Aimp2*$^{+/+}$ ($n = 3$) and *Aimp2*$^{+/-}$ ($n = 3$). White arrows indicate Ki67^{+} or BrdUrd^{+} crypt base cells, respectively. The crypts are outlined by white dashed lines (**E** and **G**). At least 30 well-oriented crypts were analyzed on 3–4 slides per mouse. **I** and **J,** immunohistochemical staining (**I**) and quantification (**J**) of cleaved caspase-3 in 20-week-old *Aimp2*$^{+/+}$ ($n = 5$) and *Aimp2*$^{+/-}$ villi ($n = 5$). White arrows, cleaved caspase-3^{+} (C-Casp3) cells in the villus. At least 30 well-oriented villi were analyzed on 3–4 slides per mouse. Scale bar, 50 μm. Student *t* test was performed, and data are the mean ± SEM. *, $P < 0.01$.

AIMP2 restricts the expansion of ISCs and their niche

To investigate which types of cells are increased in *Aimp2*$^{+/-}$ intestine, we performed qRT-PCR analysis. The expression levels of goblet and enteroendocrine cell markers (*Gob5* and *Chga*) were comparable in *Aimp2*$^{+/-}$ and *Aimp2*$^{+/+}$ mice (Fig. 3A). Consistently, PAS/H and chromogranin A (ChgA) staining showed that the frequency of goblet and enteroendocrine cells was not altered in *Aimp2*$^{+/-}$ mice (Supplementary Fig. S2I–S2L). However, PC markers (*Mmp7* and *Lyz*) and ISC markers (*Lgr5*, *Olfm4*, and *Msi1*) were significantly increased in *Aimp2*$^{+/-}$ intestines compared with *Aimp2*$^{+/+}$ (Fig. 3A), suggesting that PCs and ISCs are expanded in *Aimp2*$^{+/-}$ mice.

To determine whether hemizygous deletion of *Aimp2* resulted in the expansion of the ISC compartment, we performed PAS/H staining and immunohistochemistry for lysozyme. Consistent with the mRNA expression, the number of PCs markedly increased in *Aimp2*$^{+/-}$ intestines (5.6 ± 1.3 per crypt) compared with *Aimp2*$^{+/+}$ (3.6 ± 0.7 per crypt; Fig. 3B and C). To directly assess the number of ISCs, we crossed *Aimp2*$^{+/-}$ mice with *Lgr5-EGFP* mice (1). Immunohistochemical analysis showed that EGFP^{+} ISCs in the crypts markedly increased in *Aimp2*$^{+/-}$:*Lgr5-EGFP* mice (*Aimp2*$^{+/+}$: 3.3 ± 0.5 vs. *Aimp2*$^{+/-}$: 5.7 ± 1.3 per crypt). Moreover, the number of BrdUrd^{+}:EGFP^{+} ISCs significantly increased in the *Aimp2*$^{+/-}$:*Lgr5-EGFP* crypts (*Aimp2*$^{+/+}$: 0.9 ± 0.4 vs. *Aimp2*$^{+/-}$: 2.5 ± 0.7 per crypt; Fig. 3D and E), showing that two alleles of *Aimp2* are required to suppress the expansion of ISC compartments in the crypt.

AIMP2 inhibits Wnt/β-catenin signaling in the intestinal epithelium

To investigate the mechanism by which AIMP2 restricts the expansion of the ISC compartment, we first examined the target genes of known AIMP2-associated signaling pathways (16–18) such as FBP (*Usp29* and *Cdkn1a*), NF-κB (*Tnf*, *Gadd45b*, and *Ciap2*), and p53 (*Puma*, *Wip1*, and *Phlda3*; refs. 26–28). However, there were no significant differences in the expressions between the *Aimp2*$^{+/-}$ and *Aimp2*$^{+/+}$ intestine (data not shown), suggesting that the phenotype in *Aimp2*$^{+/-}$ intestine may not be caused by alteration of previously reported signaling.

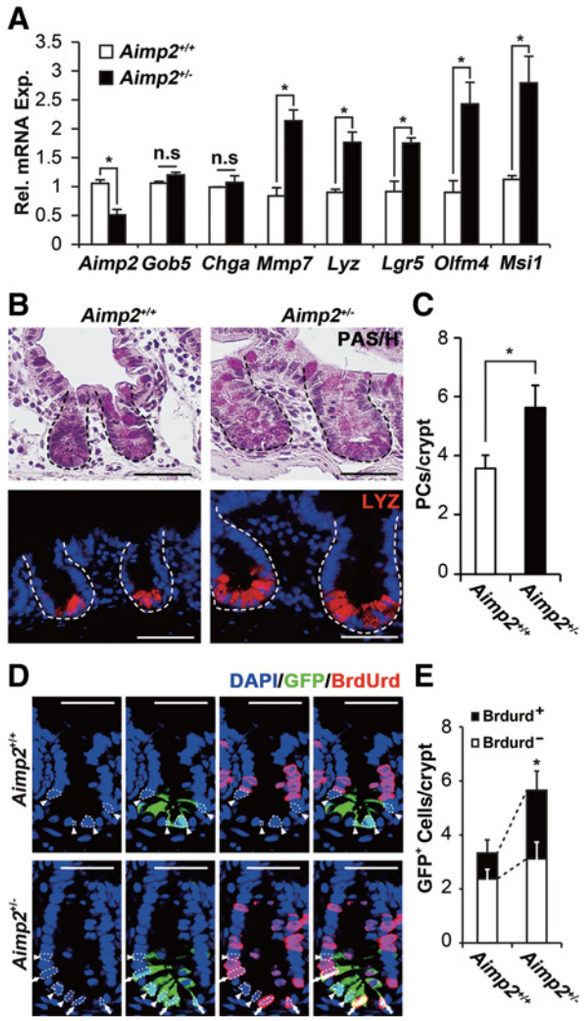

Figure 3.
Expansion of intestinal stem cell compartment in *Aimp2*$^{+/-}$ mice. **A,** mRNA expressions of different intestinal cell lineage markers in 6-week-old *Aimp2*$^{+/+}$ ($n = 4$) and *Aimp2*$^{+/-}$ ($n = 5$) intestinal epithelium. **B,** PAS/H staining and immunohistochemical staining of Lysozyme in ileums. The crypts are outlined by black or white dashed lines. **C,** quantification of lysozyme^{+} cells in *Aimp2*$^{+/+}$ ($n = 3$) and *Aimp2*$^{+/-}$ crypts ($n = 3$). **D** and **E,** immunohistochemical staining (**D**) and quantification (**E**) of GFP and BrdUrd in 6-week-old *Aimp2*$^{+/+}$*:Lgr5-EGFP* ($n = 3$) and *Aimp2*$^{+/-}$*:Lgr5-EGFP* ($n = 3$) ileums. The GFP^{+} ISCs are outlined by white dashed lines. Arrowhead and arrow indicate BrdUrd^{-}:GFP^{+} ISCs and BrdUrd^{+}:GFP^{+} ISCs, respectively. At least 30 well-oriented crypts were analyzed on 3–4 slides per mouse. Scale bar, 50 μm. Student *t* test was applied, and data are the mean ± SEM. *, $P < 0.01$.

At the crypt base, Wnt/β-catenin signaling governs the maintenance of ISCs and PCs, and uncontrolled activation of Wnt/β-catenin signaling leads to the expansion of ISC compartments (10, 29). Because the number of ISCs and PCs increased in *Aimp2*$^{+/-}$ mice, we investigated whether Wnt/β-catenin signaling was enhanced in the *Aimp2*$^{+/-}$ intestine. Consistent with increased levels of Wnt/β-catenin target genes (*Axin2*, *C-myc*, *Cd44*; Fig. 4A), immunohistochemical analysis also showed that CD44 and C-MYC–expressing cells markedly increased in *Aimp2*$^{+/-}$ crypts (Fig. 4B and C). Moreover, increased protein levels of nonphosphorylated β-catenin, AXIN2, and NKD1 also showed the enhanced Wnt/β-catenin signaling in *Aimp2*$^{+/-}$ IECs (Fig. 4D and E), suggesting that AIMP2 inhibits Wnt/β-catenin signaling.

AIMP2 binds with DVL to interrupt Dvl–Axin interaction

To investigate how AIMP2 inhibits Wnt/β-catenin signaling, we performed an *in vitro* binding assay with the major components of the canonical Wnt pathway. Intriguingly, we found that DVL bound to AIMP2 (Supplementary Fig. S3A), and confirmed with coimmunoprecipitation experiments in HCT116 cells (Fig. 5A). We then examined whether AIMP2 colocalized with DVL. Ectopic expression of AIMP2 alone showed its diffused localization in the cytoplasm. However, coexpression of AIMP2 with DVL1 led to colocalization of AIMP2 with DVL1 as a puncta (Fig. 5B). To identify the AIMP2 interaction domain in DVL, we performed domain mapping with intact DVL1 and two DVL1 mutants, ΔDEP-DVL1 and ΔDIX-DVL1. We found that the DIX domain of DVL1 bound to AIMP2 (Supplementary Fig. S3B). As DIX domain is crucial for DVL–AXIN interaction (30, 31), the binding of AIMP2 and DVL might disrupt the interaction between DVL1 and AXIN. To test this possibility, we performed coimmunoprecipitation. As expected, coexpression of AIMP2 markedly inhibited the DVL1–AXIN1 interaction (Fig. 5C). Importantly,

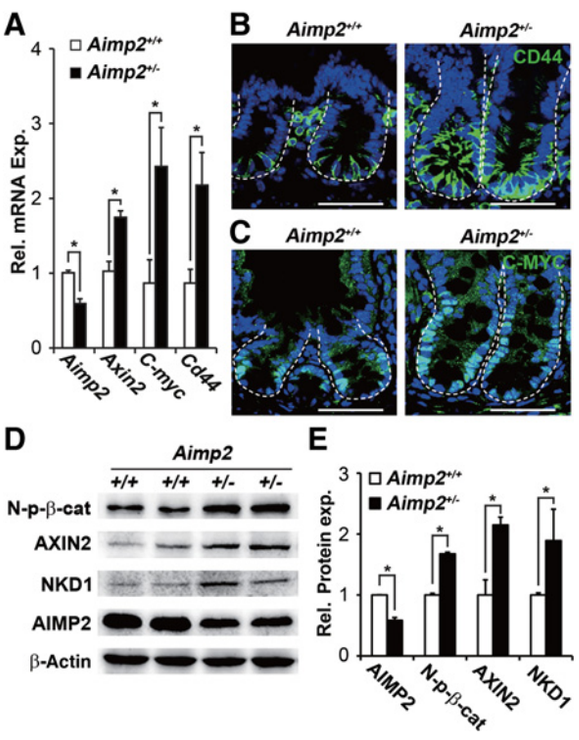

Figure 4.
Increased Wnt/β-catenin signaling in *Aimp2*$^{+/-}$ mice. **A,** mRNA expressions of Wnt/β-catenin target genes in 6-week-old *Aimp2*$^{+/+}$ ($n = 6$) and *Aimp2*$^{+/-}$ ($n = 6$) intestinal epithelium. **B** and **C,** immunohistochemical staining of CD44 (**B**) and C-MYC (**C**) in ileums. **D** and **E,** immunoblotting (**D**) and quantitative densitometry (**E**) of whole-cell extracts from 6-week-old *Aimp2*$^{+/+}$ ($n = 4$) and *Aimp2*$^{+/-}$ ($n = 4$) IECs. The crypts are outlined by white dashed lines. Scale bar, 50 μm. Student *t* test was applied, and data are the mean ± SEM. *, $P < 0.01$.

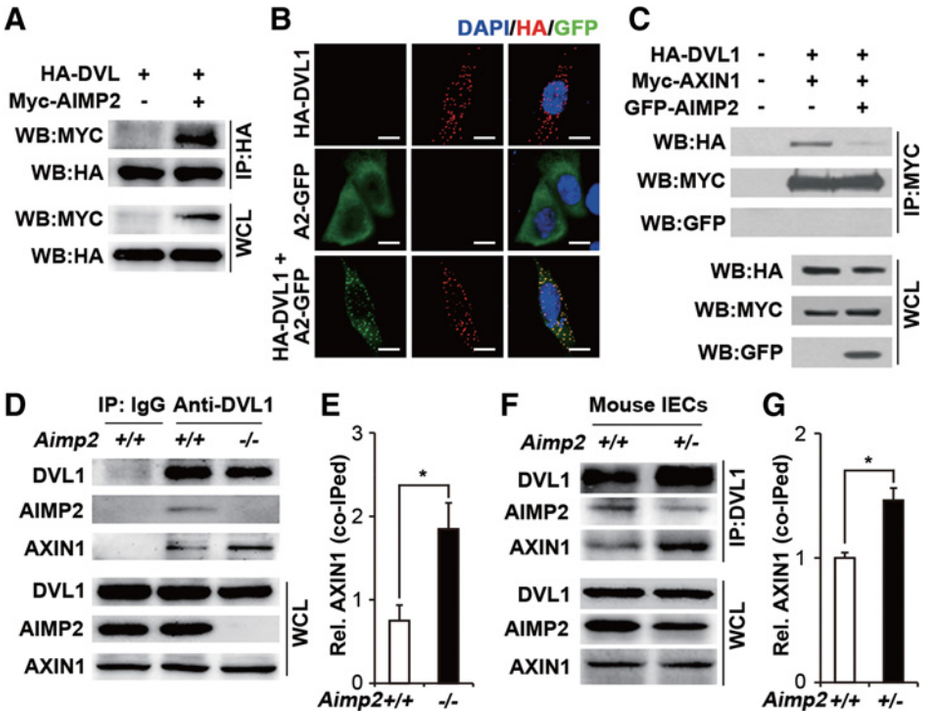

Figure 5.
AIMP2 binds with DVL to interrupt DVL–AXIN interaction. **A** and **B,** HCT116 cells were transfected with plasmids as indicated. Immunoprecipitation (**A**) using an anti-HA antibody and immunocytochemical staining (**B**) using anti-HA and GFP antibody. A2-GFP represents AIMP2-GFP. **C,** HeLa cells were transfected with plasmids as indicated, and protein was immunoprecipitated using an anti-MYC antibody. **D** and **E,** immunoprecipitation analysis (**D**) and quantitative densitometry of the co-immunoprecipitated AXIN1 (**E**) using whole cell extracts from *Aimp2*$^{+/+}$ and *Aimp2*$^{-/-}$ MEFs treated with Wnt3a for 24 hours. **F** and **G,** immunoprecipitation analysis (**F**) and quantitative densitometry of the co-immunoprecipitated (co-IPed) AXIN1 (**G**) using whole-cell extracts from 6-week-old *Aimp2*$^{+/+}$ ($n = 4$) and *Aimp2*$^{+/-}$ ($n = 4$) IECs. Scale bar, 10 μm. Student *t* test was applied, and data are the mean ± SEM. *, $P < 0.01$. At least three independent experiments were performed.

endogenous AIMP2 also interacted with endogenous DVL1, and reduction of AIMP2 significantly increased the DVL1–AXIN1 interaction in MEFs (Fig. 5D and E). We confirmed the endogenous interaction by coimmunoprecipitation using freshly isolated *Aimp2*$^{+/+}$ and *Aimp2*$^{+/-}$ IECs (Fig. 5F and G). These results suggest that AIMP2 disrupts DVL–AXIN interaction by competing with AXIN.

AIMP2 inhibits Wnt/β-catenin signaling

Because AIMP2 inhibited the DVL–AXIN interaction, we tested whether AIMP2 negatively regulated Wnt/β-catenin signaling. Overexpression of AIMP2 inhibited the activity of TOPflash, a reporter for Wnt/β-catenin signaling (Fig. 6A), the expression of the Wnt/β-catenin target genes, *AXIN2* and *NKD1* (Supplementary Fig. S3C), the accumulation of non-phosphorylated β-catenin, and the induction of AXIN2 and NKD1 after Wnt3a stimulation (Fig. 6B). Conversely, *AIMP2* knockdown (Supplementary Fig. S3D and S3E) further augmented Wnt3a-mediated increase of the TOPflash activity (Fig. 6C), the accumulation of nonphosphorylated β-catenin and the target gene expressions (Fig. 6D and Supplementary Fig. S3F). Consistently, ablation of *Aimp2* in MEFs (Supplementary Fig. S3G and S3H) increased the accumulation of nonphosphorylated β-catenin, the induction of target genes and the TOPflash activity with or without Wnt3a stimulation (Fig. 6E and Supplementary Fig. S3I and S3J). Blockade of Wnt ligand secretion by a porcupine inhibitor, IWP4 (32), revealed that the increased Wnt/β-catenin signaling in *Aimp2*$^{-/-}$ MEFs depends on Wnt ligand administration (Supplementary Fig. S3K), suggesting that *Aimp2*$^{-/-}$ MEFs were more sensitive to Wnt ligands than *Aimp2*$^{+/+}$ MEFs. Taken together, these results show that AIMP2 inhibits Wnt/β-catenin signaling by disrupting the interaction between DVL and AXIN.

Previous studies suggested that AIMP2 is involved in ubiquitination-dependent degradation of TRAF2 and p53 (17, 18) by the direct interaction. Thus, we tested whether AIMP2 modulates the Wnt/β-catenin signaling by ubiquitination of DVL1. When DVL1 was overexpressed alone or with AIMP2, there was no significant difference in DVL1 level (Fig. 5A–C). Moreover, the protein levels of DVL1 in MEFs and *Aimp2*$^{+/+}$, *Aimp2*$^{+/-}$, and even *Aimp2*$^{-/-}$ IECs were comparable, suggesting that the inhibitory role of AIMP2 on Wnt/β-catenin signaling may not depend on DVL1 degradation (Supplementary Fig. S4A–S4C). We also observed that other potential ubiquitination targets, TRAF2 or p53 (18, 19), were unaffected by reduction of AIMP2 in IECs (Supplementary Fig. S4D–S4G), indicating that the role of AIMP2 in intestine was specific to the Wnt/β-catenin signaling.

As AIMP2 associates with several E3 ligases such as IAP-1 (17) and MDM2 (18), we further tested whether AIMP2 affects the ubiquitination of β-catenin independently of destruction complex. When HeLa cells were treated with GSK-3β inhibitor (CHIR99021), AIMP2 overexpression did not induce the ubiquitination of β-catenin. In contrast, AIMP2 readily induced the ubiquitination of β-catenin when cells were stimulated with Wnt3a (Fig. 6F), suggesting that AIMP2 inhibits upstream of GSK-3β in Wnt/β-catenin signaling. Consistently, in the presence of CHIR99021, TOPflash activity (Fig. 6G and H) and *AXIN2* mRNA expression (Supplementary Fig. S4H and S4I) were not affected by AIMP2 level. Therefore, we concluded that the regulatory role of AIMP2 in Wnt/β-catenin signaling is mainly dependent on the disruption of DVL–AXIN interaction, not the direct ubiquitination.

Aimp2 gene dosages modulate the sensitivity of Wnt/β-catenin signaling

On the basis of the data from the *Aimp2*$^{+/-}$ intestine, we speculated that *Aimp2* gene dosage is important for inhibitory role of AIMP2 in Wnt/β-catenin signaling. Indeed, compared

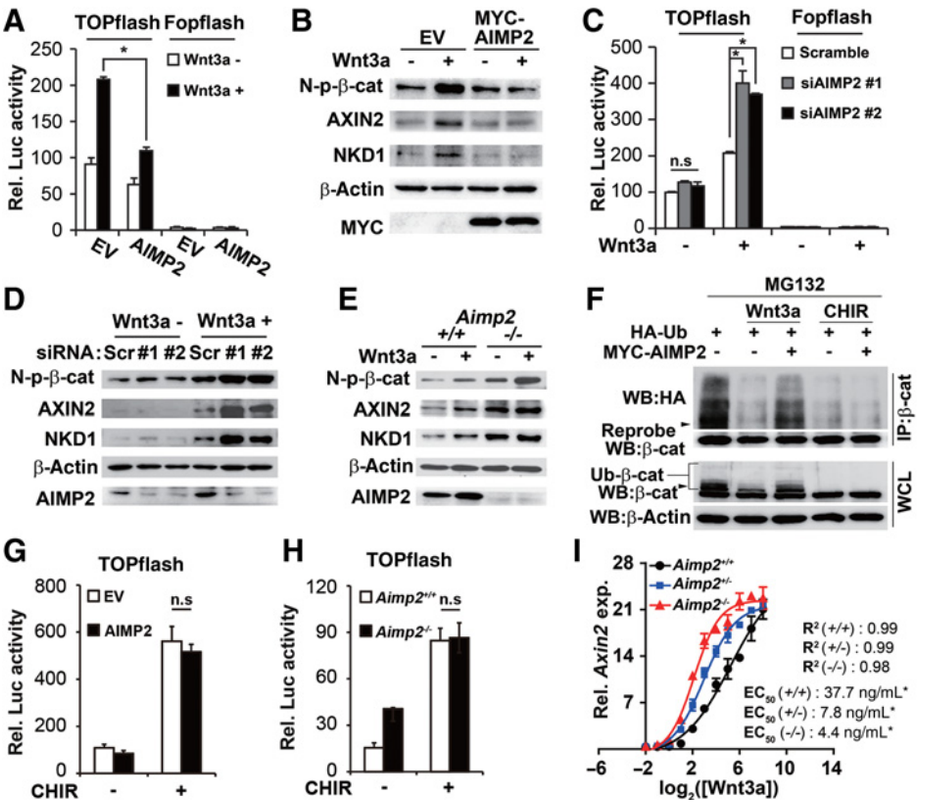

Figure 6.

AIMP2 inhibits Wnt/β-catenin signaling. **A** and **B,** TOPflash analysis (**A**) and immunoblotting (**B**) of whole-cell extracts from HeLa cells transfected with empty vector (EV) or AIMP2 expression vector, and treated with Wnt3a for 24 hours. **C** and **D,** TOPflash analysis (**C**) and immunoblotting (**D**) of HeLa cells transfected with scramble (Scr) or AIMP2 siRNAs and treated with Wnt3a for 24 hours. **E,** immunoblotting of whole cell extracts from *Aimp2*$^{+/+}$ and *Aimp2*$^{-/-}$ MEFs treated with Wnt3a for 24 hours. **F** and **G,** HeLa cells were transfected with plasmids as indicated, and protein was immunoprecipitated using anti-β-catenin antibody and immunoblotted using indicated antibodies (**F**). Black arrowheads, 100 kDa. The TOPflash activity of HeLa cells (**G**) or *Aimp2*$^{+/+}$ and *Aimp2*$^{-/-}$ MEFs (**H**) were measured in the absence or presence of GSK-3β inhibitor (CHIR99021, Stemgent). **I,** dose–response curve to Wnt3a of MEFs. The cells were pretreated with porcupine inhibitor (IWP4, Stemgent) for 24 hours and stimulated with Wnt3a for 12 hours. **A, C, G,** and **H,** Student *t* test was applied, and data are the mean ± SEM. *, $P < 0.01$. **I,** ANOVA on effective concentration (EC_{50}) value was applied, and data are the mean ± SEM. *, $P < 0.01$. At least three independent experiments were performed.

with *Aimp2*$^{+/+}$, *Aimp2*$^{+/-}$ MEFs showed increased TOPflash activity and expressed higher levels of *Axin2* and *Nkd1*. In addition, the increase was further augmented in *Aimp2*$^{-/-}$ MEFs (Supplementary Fig. S3I and S3J), suggesting that hemizygous expression of AIMP2 is insufficient to inhibit Wnt/β-catenin signaling. To further examine the dosage effect of AIMP2, we measured effective concentration (EC_{50})of Wnt3a using MEFs. As expected, the EC_{50} significantly decreased when *Aimp2* dosage reduced (Fig. 6I)

To confirm the dosage effects of AIMP2 in Wnt/β-catenin signaling, we performed organoid formation assays (22) in the presence of Roof plate–specific spondin 1 (R-spondin-1) using IECs from E18.5 *Aimp2*$^{+/+}$, *Aimp2*$^{+/-}$, and *Aimp2*$^{-/-}$ mouse embryos. Binding of R-spondin-1 to LGR4/5 inhibits the RNF43 and ZNRF3 E3 ligases and activates Wnt/β-catenin signaling in ISCs (33). On day 3 of culture, the formation of intestinal organoids was negatively correlated with *Aimp2* gene dosage, especially at very low concentrations of R-spondin-1 (Fig. 7A and B). However, in the absence of R-spondin-1, no living organoids were present, regardless of genotype, suggesting that AIMP2 plays an inhibitory role in Wnt/β-catenin signaling downstream of RNF43 and ZNRF3.

Consistently, the expression of Wnt/β-catenin target genes and ISC markers (Fig. 7C), the growth (Supplementary Fig. S5A and S5B) and the proliferation (Fig. 7D and E) of organoids were negatively correlated with the *Aimp2* gene dosage. Together, these results support the idea that AIMP2 inhibits the activity of Wnt/β-catenin signaling in IECs in a gene dosage–dependent manner.

Discussion

Because an adequate level of Wnt/β-catenin signaling activity is critical for maintaining ISCs, it is important to understand the mechanism that the Wnt/β-catenin signaling activity is regulated in the intestine. Here, we show that AIMP2 binds to DVL, a key component of the Wnt/β-catenin signaling pathway and inhibits the interaction between DVL and AXIN. The inhibitory effect of AIMP2 on Wnt/β-catenin signaling is negatively correlated with the *Aimp2* gene dosage. Intriguingly, hemizygous expression of AIMP2 in the intestine was insufficient for proper control of

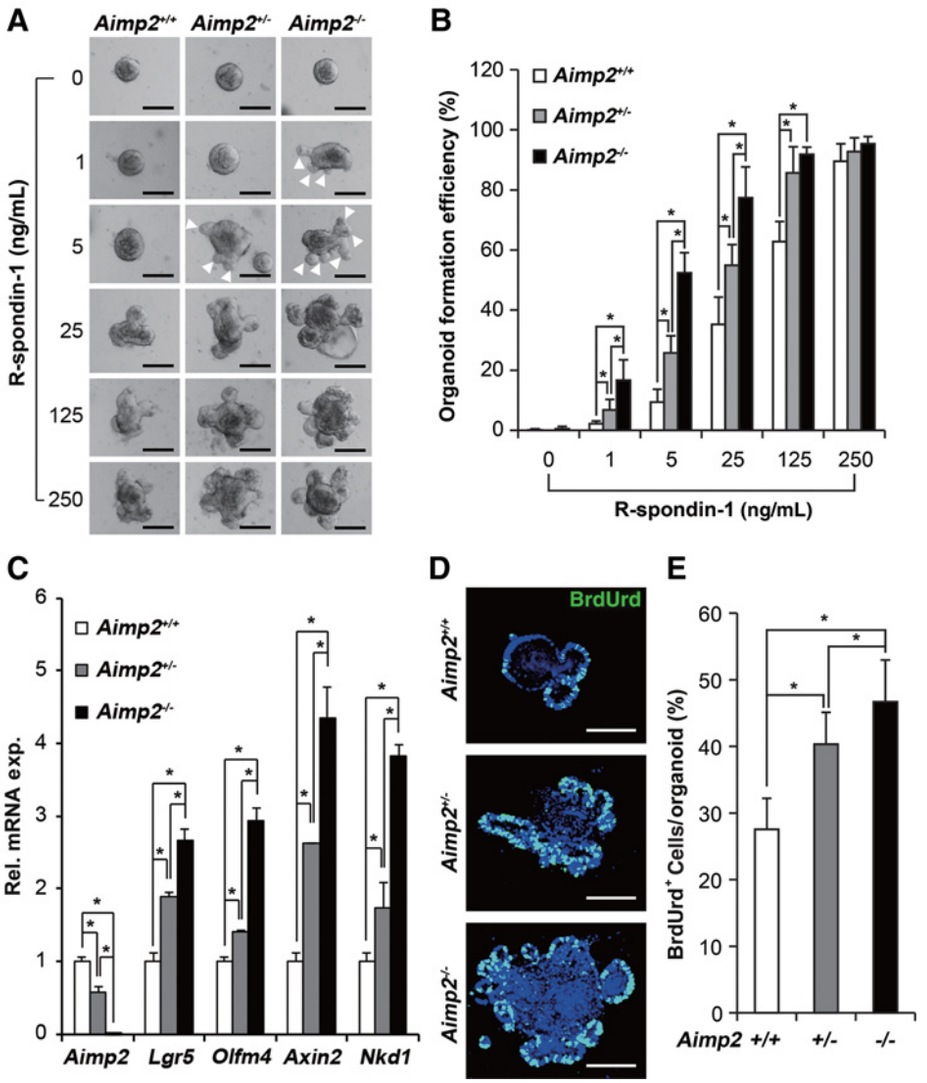

Figure 7.
Effects of *Aimp2* gene dosage on the sensitivity of intestinal organoids to Wnt/β-catenin signaling. **A** and **B,** stereomicroscopic images (**A**) and organoid formation efficiency (**B**) of $Aimp2^{+/+}$, $Aimp2^{+/-}$, and $Aimp2^{-/-}$ intestinal organoids. Arrows, budding of organoids. Two-hundred crypts were seeded, and budding organoids were counted as live organoids at day 3 of culture. **C,** mRNA expressions of organoids at day 3 of culture with 25 ng/mL R-spondin-1. **D** and **E,** immunohistochemical staining (**D**) and quantification (**E**) of BrdUrd in organoids. At least 10 organoids were analyzed for each genotype. Scale bar, 100 μm. ANOVA was performed, and data are the mean ± SEM. *, $P < 0.01$. At least three independent experiments were performed.

Wnt/β-catenin signaling activity, which is pivotal in maintaining an adequate ISC pool size in the crypts. Collectively, our data show that AIMP2 is an important regulator that controls the activity of Wnt/β-catenin signaling, the ISC populations, and eventually the tumorigenesis in the crypts.

In the intestinal crypts, PCs and cryptal myofibroblasts have been considered the major sources of canonical Wnt ligands (2, 9). However, a recent study showed that Wnt ligands produced by unknown cellular sources are sufficient to support ISCs in the absence of PCs and myofibroblasts (34), indicating that intestinal crypts are awash with Wnt ligands. Despite the surplus Wnt ligands in the crypts, Wnt/β-catenin signaling is not fully activated in ISCs and transit-amplifying (TA) cells, suggesting that a number of negative regulators restrict the activation of Wnt/β-catenin signaling. Recently emerged Wnt agonist, R-spondins likely diffuse from their unknown cellular source to activate Wnt/β-catenin signaling in surrounding epithelial cells, including ISCs. In the current study, we found that the expression of AIMP2 negatively correlated with sensitivity to R-spondin-1, suggesting that AIMP2 prevents unwanted activation of ISCs by regulating the activity of Wnt/β-catenin signaling.

Various receptors, such as receptor tyrosine kinase receptors, Toll-like receptors, and TNF receptors, require high-order assemblies of intracellular signaling factors (35). Because signalosome formation requires oligomerization, the receptors show a sigmoidal response to ligand concentration, reducing biologic noise or unwanted activation. Wnt ligand-receptor binding also leads to the clustering of Frizzled and LRP6 and the polymerization of DVL. DVL self-assembles through its DIX domain and forms interaction platforms for low-affinity binding partners such as AXIN (31). In our study, AIMP2 competed with AXIN for binding to the DIX domain of DVL. Intriguingly, the activity of Wnt/β-catenin signaling negatively correlated with the *Aimp2* gene dosage, suggesting that AIMP2 expression level is crucial for regulation of the interaction between DVL and AXIN. Competition with AXIN might create a sharp sigmoidal response to Wnt ligands in the presence of R-spondin-1, which would provide a mechanism for reducing biologic noise or unwanted activation of Wnt/β-catenin signaling in cryptic epithelial cells.

Why do *Aimp2*$^{+/-}$ crypts exhibit haploinsufficiency? AIMP2 serves as a scaffolding protein for the assembly of several different ARSs into the multi-tRNA synthetase complex (11). If AIMP2 is predominantly trapped in multi-synthetase complexes, a limited amount of "free" AIMP2 is available to participate in nontranslational activities, such as interacting with FBP, p53, and TRAF2 (16–18). Thus, in *Aimp2*$^{+/-}$ mice, the amount of AIMP2 could be insufficient to support its noncanonical functions as a signaling modulator. Our data suggest another mechanism for AIMP2 haploinsufficiency, in which AIMP2 modulates Wnt/β-catenin signaling in the intestine by interfering with the DVL–AXIN interaction. On the other hand, recent studies have reported that PARKIN degrades AIMP2 in dopaminergic neurons and that disruption of PARKIN results in the accumulation of AIMP2, potentially causing neurodegenerative disease (36, 37). Overall, these observations raise the intriguing possibility that the cellular level of AIMP2 is important in various pathophysiologic contexts.

The key cellular events promoting tumor initiation include uncontrolled cell proliferation. LOH of *Apc*, a process directly linked to tumor initiation in *Apc*$^{Min/+}$ mice can occur in highly proliferative cells due to dysregulated cell cycle (25, 38). Thus, the expanded ISC compartment and IEC proliferation might be responsible for increased tumorigenesis in *Aimp2*$^{+/-}$:*Apc*$^{Min/+}$ mice. These findings are consistent with earlier report using AOM/DSS colitis–associated tumor model with increased number of polyps in the *Aimp2*$^{+/-}$ colon (19). Furthermore, the increased ACF in *Aimp2*$^{+/-}$:*Apc*$^{Min/+}$ mice suggests that intestinal AIMP2 is essential for inhibiting adenoma initiation. Collectively, our current study revealed a critical role of AIMP2 in modulating intestinal Wnt/β-catenin signaling and tumorigenesis. Disruption of DVL–AXIN interaction by AIMP2 fine-tunes the Wnt/β-catenin signaling activity in intestinal crypts. Our observation will provide a better understanding of regulation of intestinal Wnt signaling and tumorigenesis.

Disclosure of Potential Conflicts of Interest

No potential conflicts of interest were disclosed.

Writing Assistance

The edit was performed by professional editors at Editage, a division of Cactus Communications, and was funded by the Institute for Basic Science of Seoul National University.

Authors' Contributions

Conception and design: M.K. Yum, H.-A. Kim, Y.-Y. Kim, J.M. Han
Development of methodology: M.K. Yum
Acquisition of data (provided animals, acquired and managed patients, provided facilities, etc.): M.K. Yum, J.-S. Kang, A.-E. Lee, Y.-W. Jo, H.-A. Kim, Y.-Y. Kim, E.B. Lee, J.M. Han
Analysis and interpretation of data (e.g., statistical analysis, biostatistics, computational analysis): M.K. Yum, J.-S. Kang, A.-E. Lee, Y.-W. Jo, E.B. Lee, J.M. Han, Y.-Y. Kong
Writing, review, and/or revision of the manuscript: M.K. Yum, J.Y. Seo, J. Seong, J.-H. Kim, Y.-Y. Kong
Administrative, technical, or material support (i.e., reporting or organizing data, constructing databases): J. Seong, J.-H. Kim
Study supervision: S. Kim, Y.-Y. Kong

Acknowledgments

The authors thank Bon-Kyung Koo and Doyeun Kim for suggesting useful methods for this study and Inkuk Park for helpful comments for manuscript preparation.

Grant Support

This work was supported by Basic Science Research Program (NRF-2014R1A2A1A10052675), Bio & Medical Technology Development Program (NRF-2011-0019269), Korea Mouse Phenotyping Project (NRF-2014M3A9D5A01073930), and a Global Frontier Project grant (NRF-2010-0029780) of the Ministry of Science, ICT and Future of the National Research Foundation (Y.-Y. Kong), funded by Korean government.

The costs of publication of this article were defrayed in part by the payment of page charges. This article must therefore be hereby marked *advertisement* in accordance with 18 U.S.C. Section 1734 solely to indicate this fact.

Received December 8, 2015; revised March 30, 2016; accepted May 3, 2016; published OnlineFirst June 4, 2016.

References

1. Barker N, van Es JH, Kuipers J, Kujala P, van den Born M, Cozijnsen M, et al. Identification of stem cells in small intestine and colon by marker gene Lgr5. Nature 2007;449:1003–7.
2. Sato T, van Es JH, Snippert HJ, Stange DE, Vries RG, van den Born M, et al. Paneth cells constitute the niche for Lgr5 stem cells in intestinal crypts. Nature 2011;469:415–8.
3. Clevers H, Nusse R. Wnt/beta-catenin signaling and disease. Cell 2012;149:1192–205.
4. Cadigan KM, Peifer M. Wnt signaling from development to disease: insights from model systems. Cold Spring Harb Perspect Biol 2009;1:a002881.
5. Korinek V, Barker N, Moerer P, van Donselaar E, Huls G, Peters PJ, et al. Depletion of epithelial stem-cell compartments in the small intestine of mice lacking Tcf-4. Nat Genet 1998;19:379–83.
6. Pinto D, Gregorieff A, Begthel H, Clevers H. Canonical Wnt signals are essential for homeostasis of the intestinal epithelium. Genes Dev 2003;17:1709–13.
7. van de Wetering M, Sancho E, Verweij C, de Lau W, Oving I, Hurlstone A, et al. The beta-catenin/TCF-4 complex imposes a crypt progenitor phenotype on colorectal cancer cells. Cell 2002;111:241–50.
8. Barker N, Ridgway RA, van Es JH, van de Wetering M, Begthel H, van den Born M, et al. Crypt stem cells as the cells-of-origin of intestinal cancer. Nature 2009;457:608–11.
9. Farin HF, Van Es JH, Clevers H. Redundant sources of Wnt regulate intestinal stem cells and promote formation of Paneth cells. Gastroenterology 2012;143:1518–29.
10. Koo BK, Spit M, Jordens I, Low TY, Stange DE, van de Wetering M, et al. Tumour suppressor RNF43 is a stem-cell E3 ligase that induces endocytosis of Wnt receptors. Nature 2012;488:665–9.
11. Quevillon S, Robinson JC, Berthonneau E, Siatecka M, Mirande M. Macromolecular assemblage of aminoacyl-tRNA synthetases: identification of protein-protein interactions and characterization of a core protein. J Mol Biol 1999;285:183–95.
12. Kim S, You S, Hwang D. Aminoacyl-tRNA synthetases and tumorigenesis: more than housekeeping. Nat Rev Cancer 2011;11:708–18.
13. Park BJ, Kang JW, Lee SW, Choi SJ, Shin YK, Ahn YH, et al. The haploinsufficient tumor suppressor p18 upregulates p53 via interactions with ATM/ATR. Cell 2005;120:209–21.
14. Wakasugi K, Slike BM, Hood J, Ewalt KL, Cheresh DA, Schimmel P. Induction of angiogenesis by a fragment of human tyrosyl-tRNA synthetase. J Biol Chem 2002;277:20124–6.
15. Ko YG, Park H, Kim T, Lee JW, Park SG, Seol W, et al. A cofactor of tRNA synthetase, p43, is secreted to up-regulate proinflammatory genes. J Biol Chem 2001;276:23028–33.
16. Kim MJ, Park BJ, Kang YS, Kim HJ, Park JH, Kang JW, et al. Downregulation of FUSE-binding protein and c-myc by tRNA synthetase cofactor p38 is required for lung cell differentiation. Nat Genet 2003;34:330–6.

17. Choi JW, Kim DG, Park MC, Um JY, Han JM, Park SG, et al. AIMP2 promotes TNFalpha-dependent apoptosis via ubiquitin-mediated degradation of TRAF2. J Cell Sci 2009;122:2710–5.
18. Han JM, Park BJ, Park SG, Oh YS, Choi SJ, Lee SW, et al. AIMP2/p38, the scaffold for the multi-tRNA synthetase complex, responds to genotoxic stresses via p53. Proc Natl Acad Sci U S A 2008;105:11206–11.
19. Choi JW, Um JY, Kundu JK, Surh YJ, Kim S. Multidirectional tumor-suppressive activity of AIMP2/p38 and the enhanced susceptibility of AIMP2 heterozygous mice to carcinogenesis. Carcinogenesis 2009;30: 1638–44.
20. Kim JY, Kang YS, Lee JW, Kim HJ, Ahn YH, Park H, et al. p38 is essential for the assembly and stability of macromolecular tRNA synthetase complex: implications for its physiological significance. Proc Natl Acad Sci U S A 2002;99:7912–6.
21. Flint N, Cove FL, Evans GS. A low-temperature method for the isolation of small-intestinal epithelium along the crypt-villus axis. Biochem J 1991; 280:331–4.
22. Sato T, Vries RG, Snippert HJ, van de Wetering M, Barker N, Stange DE, et al. Single Lgr5 stem cells build crypt-villus structures *in vitro* without a mesenchymal niche. Nature 2009;459:262–5.
23. Moser AR, Pitot HC, Dove WF. A dominant mutation that predisposes to multiple intestinal neoplasia in the mouse. Science 1990;247:322–4.
24. Takayama T, Katsuki S, Takahashi Y, Ohi M, Nojiri S, Sakamaki S, et al. Aberrant crypt foci of the colon as precursors of adenoma and cancer. N Engl J Med 1998;339:1277–84.
25. Haigis KM, Caya JG, Reichelderfer M, Dove WF. Intestinal adenomas can develop with a stable karyotype and stable microsatellites. Proc Natl Acad Sci U S A 2002;99:8927–31.
26. Zhang J, Chen QM. Far upstream element binding protein 1: a commander of transcription, translation and beyond. Oncogene 2013;32:2907–16.
27. Guma M, Stepniak D, Shaked H, Spehlmann ME, Shenouda S, Cheroutre H, et al. Constitutive intestinal NF-kappaB does not trigger destructive inflammation unless accompanied by MAPK activation. J Exp Med 2011;208:1889–900.
28. Brady CA, Jiang D, Mello SS, Johnson TM, Jarvis LA, Kozak MM, et al. Distinct p53 transcriptional programs dictate acute DNA-damage responses and tumor suppression. Cell 2011;145:571–83.
29. Andreu P, Colnot S, Godard C, Gad S, Chafey P, Niwa-Kawakita M, et al. Crypt-restricted proliferation and commitment to the Paneth cell lineage following Apc loss in the mouse intestine. Development 2005; 132:1443–51.
30. Kishida S, Yamamoto H, Hino S, Ikeda S, Kishida M, Kikuchi A. DIX domains of Dvl and axin are necessary for protein interactions and their ability to regulate beta-catenin stability. Mol Cell Biol 1999;19:4414–22.
31. Schwarz-Romond T, Fiedler M, Shibata N, Butler PJ, Kikuchi A, Higuchi Y, et al. The DIX domain of Dishevelled confers Wnt signaling by dynamic polymerization. Nat Struct Mol Biol 2007;14:484–92.
32. Chen B, Dodge ME, Tang W, Lu J, Ma Z, Fan CW, et al. Small molecule-mediated disruption of Wnt-dependent signaling in tissue regeneration and cancer. Nat Chem Biol 2009;5:100–7.
33. de Lau W, Peng WC, Gros P, Clevers H. The R-spondin/Lgr5/Rnf43 module: regulator of Wnt signal strength. Genes Dev 2014;28:305–16.
34. San Roman AK, Jayewickreme CD, Murtaugh LC, Shivdasani RA. Wnt secretion from epithelial cells and subepithelial myofibroblasts is not required in the mouse intestinal stem cell niche *in vivo*. Stem Cell Rep 2014;2:127–34.
35. Wu H. Higher-order assemblies in a new paradigm of signal transduction. Cell 2013;153:287–92.
36. Ko HS, von Coelln R, Sriram SR, Kim SW, Chung KK, Pletnikova O, et al. Accumulation of the authentic parkin substrate aminoacyl-tRNA synthetase cofactor, p38/JTV-1, leads to catecholaminergic cell death. J Neurosci 2005;25:7968–78.
37. Lee Y, Karuppagounder SS, Shin JH, Lee YI, Ko HS, Swing D, et al. Parthanatos mediates AIMP2-activated age-dependent dopaminergic neuronal loss. Nat Neurosci 2013;16:1392–400.
38. Aoki K, Tamai Y, Horiike S, Oshima M, Taketo MM. Colonic polyposis caused by mTOR-mediated chromosomal instability in Apc+/Delta716 Cdx2+/− compound mutant mice. Nat Genet 2003;35:323–30.